

Catalysis of an S_N2 pathway by geometric preorganization

<https://doi.org/10.1038/s41586-024-07811-4>

Gabriel J. Lovinger^{1,2}, Marcus H. Sak^{1,2} & Eric N. Jacobsen¹✉

Received: 23 February 2024

Accepted: 10 July 2024

Published online: 18 July 2024

 Check for updates

Bimolecular nucleophilic substitution (S_N2) mechanisms occupy a central place in the historical development and teaching of the field of organic chemistry¹. Despite the importance of S_N2 pathways in synthesis, catalytic control of ionic S_N2 pathways is rare and notably uncommon even in biocatalysis^{2,3}, reflecting the fact that any electrostatic interaction between a catalyst and the reacting ion pair necessarily stabilizes its charge and, by extension, reduces polar reactivity. Nucleophilic halogenase enzymes navigate this tradeoff by desolvating and positioning the halide nucleophile precisely on the S_N2 trajectory, using geometric preorganization to compensate for the attenuation of nucleophilicity⁴. Here we show that a small-molecule (646 Da) hydrogen-bond-donor catalyst accelerates the S_N2 step of an enantioselective Michaelis–Arbuzov reaction by recapitulating the geometric preorganization principle used by enzymes. Mechanistic and computational investigations show that the hydrogen-bond donor diminishes the reactivity of the chloride nucleophile yet accelerates the rate-determining dealkylation step by reorganizing both the phosphonium cation and the chloride anion into a geometry that is primed to enter the S_N2 transition state. This new enantioselective Arbuzov reaction affords highly enantioselective access to an array of *H*-phosphinates, which are in turn versatile *P*-stereogenic building blocks amenable to myriad derivatizations. This work constitutes, to our knowledge, the first demonstration of catalytic enantiocontrol of the phosphonium dealkylation step, establishing a new platform for the synthesis of *P*-stereogenic compounds.

Bimolecular S_N2 pathways between charged species generally proceed more rapidly in polar aprotic solvents than in protic solvents. For example, the reaction of azide with trimethylsulfonium is decelerated by 10⁵ in methanol relative to the same reaction in acetone⁵ (Fig. 1a). The classical interpretation is that H-bonding interactions from protic solvent molecules stabilize the ionic reactants more strongly than the partially charged S_N2 transition state, leading to a higher activation barrier^{1,5}. Selective catalysis of reactions involving ionic S_N2 mechanisms must overcome the fact that any explicit electrostatic interactions with an ion pair are likely to stabilize the reactants relative to the transition state and result in rate attenuation rather than acceleration.

Of the few enzyme classes that promote S_N2 mechanisms, most use general acid–base catalysis to activate uncharged nucleophiles or electrophiles². An alternative mode of catalysis has been documented for the nucleophilic halogenase 5'-fluoro-5'-deoxyadenosine synthase (FDAS), which promotes fluoride (or chloride) displacement on a cationic S-adenosyl methionine (SAM)⁶ (Fig. 1b). Solid-state X-ray structural characterization (Fig. 1b), along with stereochemical, theoretical and kinetic studies, have established that the enzyme effects rate acceleration of around 10⁶ by the halide-binding active site (1) precisely positioning the halide in a collinear relationship to the

leaving group^{6–8} and (2) providing a ‘halide hole’ to offset the energetic penalty for desolvation of the nucleophile from water⁴. In this enzymatic mechanism, electrostatic stabilization of the transition state relative to the ground state is neither necessary nor sufficient for rate acceleration⁹; rather, the enzyme active site is preorganized to stabilize a ‘near attack’ ground-state conformation that resembles the transition state geometrically¹⁰. The reliance on ground-state preorganization is necessary because electrostatic interactions are more thermodynamically favourable with the fully charged ground state than with the activated complex.

We envisioned a biomimetic approach to designing small-molecule catalysts for ionic S_N2 mechanisms, guided by the FDAS structure–mechanism relationship. Enzyme-mimetic small-molecule organocatalytic systems have been documented to achieve rate acceleration by charge stabilization of the transition state through noncovalent interactions^{11,12} or to recapitulate enzyme-like levels of stereodifferentiation^{13–15}, yet none, to our knowledge, has explicitly leveraged the enzymatic principle of geometric ground-state preorganization. We posited that successful catalysis is practicable if, similar to FDAS, a catalyst could (1) precisely preorganize an ion pair into a geometric configuration primed for S_N2 nucleophilic substitution and (2) provide the immediate solvation shell for the nucleophile (Fig. 1c).

¹Department of Chemistry and Chemical Biology, Harvard University, Cambridge, MA, USA. ²These authors contributed equally: Gabriel J. Lovinger, Marcus H. Sak. ✉e-mail: jacobsen@chemistry.harvard.edu

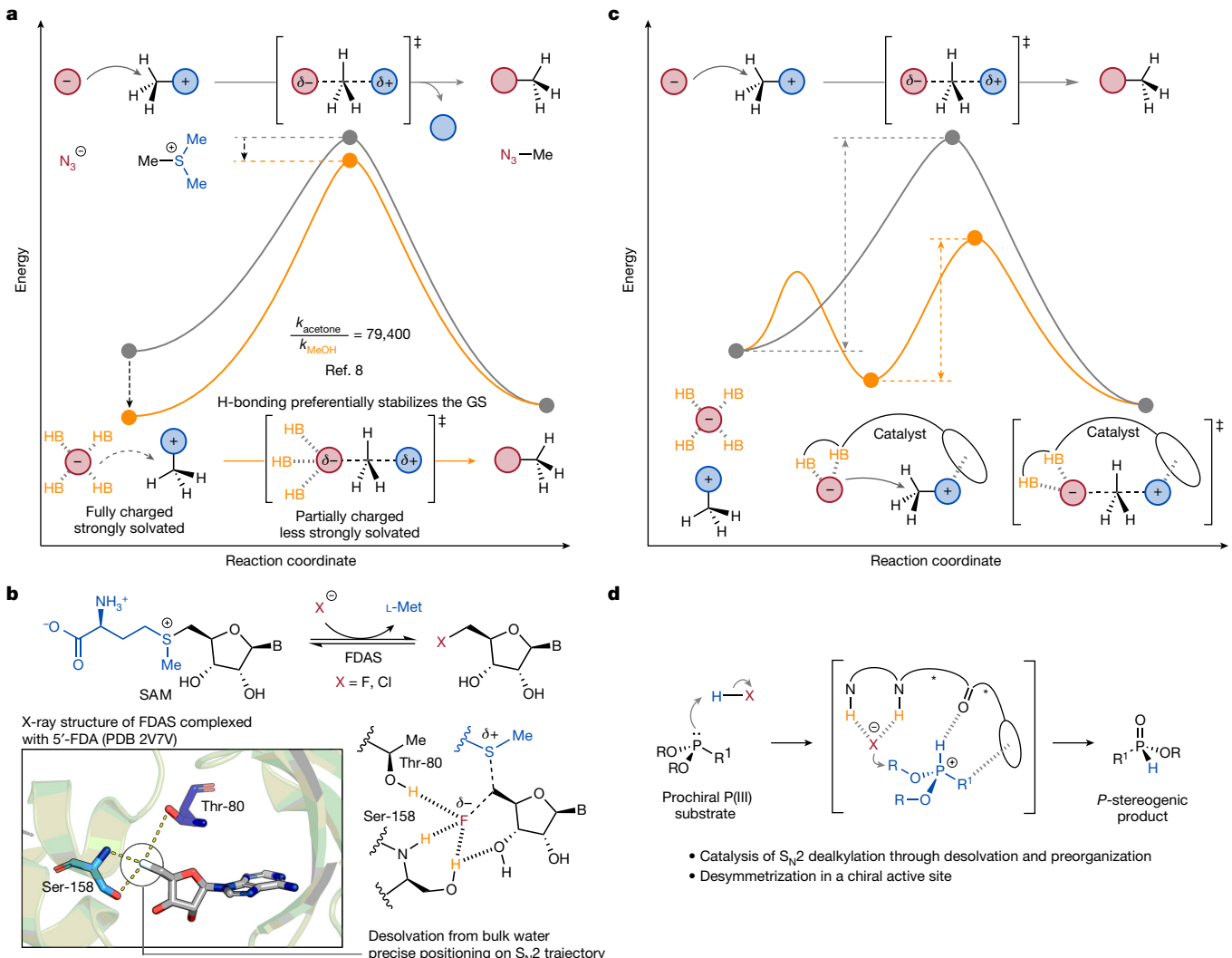


Fig. 1 | Applying enzymatic strategies to the catalysis of ionic S_N2 mechanisms. **a**, Qualitative potential energy surfaces for an S_N2 step with (orange) and without (grey) hydrogen bonding from protic solvent. **b**, FDAS: an enzymatic exemplar of nucleophile desolvation and preorganization for the catalysis of S_N2. The X-ray crystal structure of the active site bound to the product 5-fluorodeoxyadenosine is shown (PDB 2V7V)^{7,8}. **c**, Qualitative potential

energy surfaces for an S_N2 step showing the energetic consequences of substrate desolvation and preorganization, leading to an overall lower reaction barrier. **d**, Design concept for accelerating S_N2 reaction with a dual HBD catalyst, whereby a desymmetrizing nucleophilic substitution in the chiral active site affords a *P*-stereogenic product.

Based on previous work in which dual-hydrogen-bond-donor (HBD) organocatalysts were shown to control the reactions of pre-generated ion pairs^{16,17}, we considered that an appropriate adaptation in the *tert*-leucine–arylpyrrolidine HBD family might fulfil both criteria, apart from providing a chiral environment for enantioinduction^{18–22}. As a reaction platform to probe our catalytic hypothesis, we selected the Michaelis–Arbuzov reaction^{23–25}. The key step in the Arbuzov reaction is the S_N2 dealkylation of a phosphonium intermediate, an elementary step that also underpins a broad manifold of other synthetically important reactions of organophosphorus compounds. Thus, achieving catalytic enantiocontrol over this step could unlock catalytic *P*-asymmetric variants of reactions such as the Appel, Staudinger and Pudovik reactions^{26–28}. The proposed transformation starts from an achiral P(III) species with two identical alkoxy substituents that present enantiotopic sites for S_N2 dealkylation on formation of the tetrahedral phosphonium cation (Fig. 1d). If the S_N2 step is turnover-limiting, achieving high selectivity would further require that the catalyst accelerates the S_N2 step over the racemic uncatalysed reaction. Here we demonstrate that a precisely designed chiral HBD accelerates S_N2 dealkylation of phosphonium halide ion pair

intermediates in highly enantioselective Michaelis–Arbuzov reactions (Fig. 1c). The resulting *H*-phosphinate products are versatile intermediates for the preparation of stereogenic-at-phosphorus(V) compounds^{29–31}.

Reaction development

An empirical survey of variants of the Arbuzov reaction with chiral HBD catalysts showed promising enantioselectivity for the dealkylation of dibenzyl phenylphosphonite **2a** with HCl (Fig. 2a). Thiourea **1c** promoted the model reaction with higher enantioselectivities than its squaramide (**1a**) or urea (**1b**) counterparts (Fig. 2a). Furthermore, the size of the (poly)aromatic substituent as well as α -quaternary substitution at the pyrrolidine correlated positively with enantioselectivity. Ultimately, we found that thiourea **1g** bearing a 2-phenanthryl substituent promoted dealkylation in 90% enantiomeric excess (e.e.) and quantitative yield. Although catalyst optimization studies were performed using two equivalents of HCl in methyl *tert*-butyl ether (MTBE), measurable enhancements in enantioselectivity were achieved by changing the reaction solvent to toluene (Fig. 2b, entry 1), using a

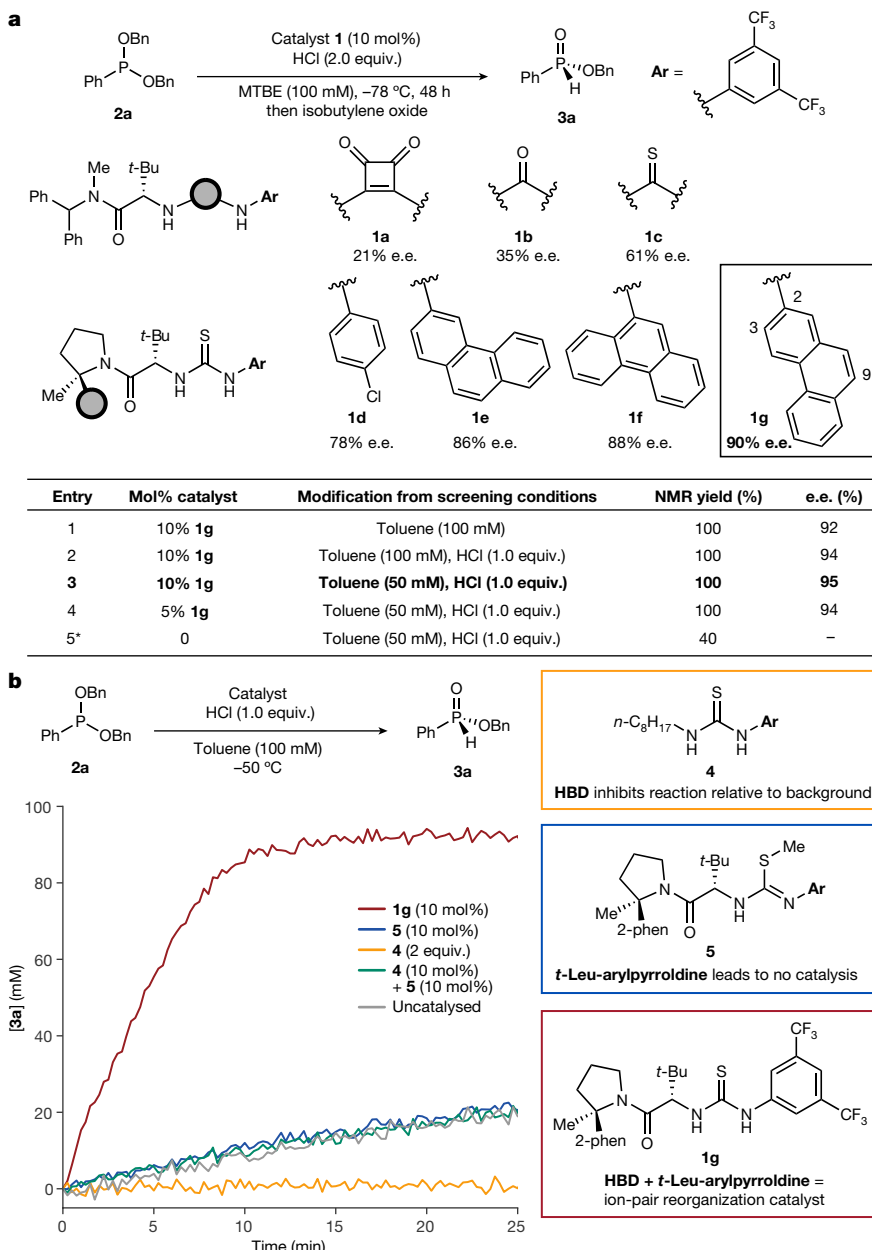


Fig. 2 | Reaction discovery and isolation of catalyst components. Yields were quantified by ¹H NMR relative to an internal standard. MTBE, methyl *tert*-butyl ether. **a**, HBD catalyst survey for enantioselective dealkylation of phosphonite **2a** and optimization of reaction conditions. The asterisk indicates

the reaction was quenched with TMSCHN₂ in Et₂O (1.5 equiv.) and the yield was quantified by quantitative ³¹P NMR. **b**, Kinetic studies probing the role of the HBD and t-Leu-arylpiperidine domains in rate acceleration. Reaction progress was monitored by following product **3a** formation using *in situ* infrared spectroscopy.

single equivalent of HCl (entry 2), and diluting the reaction mixture to 50 mM (entry 3) to furnish **3a** in 95% e.e.

Mechanistic investigations

Catalyst **1g** was found to accelerate the reaction of **2a** by a factor of 30 relative to the uncatalysed pathway (Supplementary Fig. 13). As a first step towards explaining the mechanism of catalysis, and intrigued by the possibility that promotion of the S_N2 step in a manner similar to FDAS might underlie the observed acceleration, we made simple synthetic modifications to **1g** to isolate its anion-binding (halide hole) domain from the putative cation-binding t-Leu-arylpiperidine domain (Fig. 2b). The simple anion-binding variant **4** was constructed by replacing the t-Leu-arylpiperidine moiety with an *n*-octyl group and, when used in superstoichiometric amounts to mitigate uncatalysed

background reactivity, was found to inhibit the dealkylation reaction below the rate of the background reaction (Fig. 2b, yellow versus grey traces). Thus, simple thiourea analogues of catalyst **1g** mimic protic solvents in their ability to inhibit ion-pair collapse. To probe the role of the isolated t-Leu-arylpiperidine domain in catalysis, variant **5** was synthesized by *S*-methylation of the thiourea, thereby removing the dual-HBD properties of catalyst **1g**. Compound **5** induced no rate acceleration compared with the background reaction (Fig. 2b, blue). Combining 10 mol% each of **4** and **5** also did not result in rate acceleration compared with the background. Taken together, these observations provide compelling evidence that the presence of both domains as well as their precise relative spatial orientation as in **1g** are necessary for catalysis.

We undertook a systematic mechanistic investigation to probe the identity and molecular composition of the turnover-limiting and

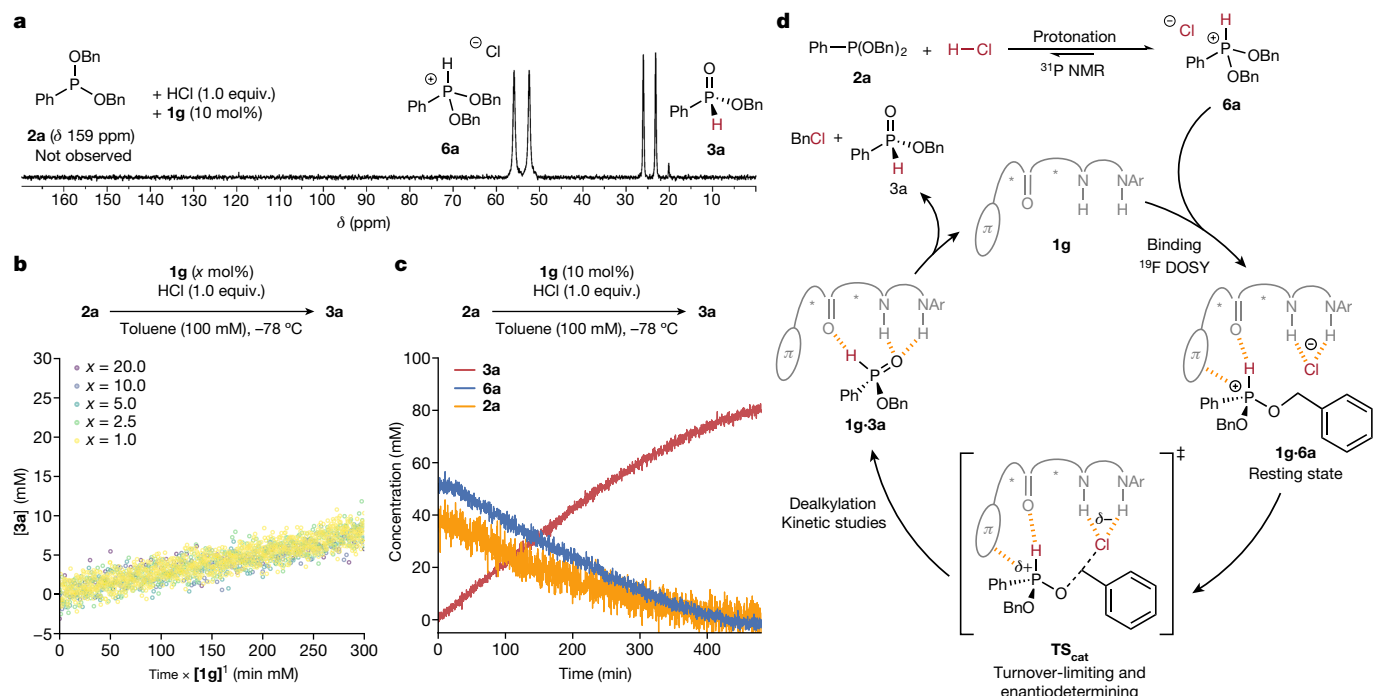


Fig. 3 | Mechanistic studies. **a**, Reaction monitoring by ^{31}P NMR. The reaction was conducted at 50 mM concentration in toluene- d_8 at -70°C . **b**, Kinetic studies to determine the order of catalyst **1g** by varying catalyst loading. Reaction progress was monitored by following product **3a** formation using *in situ*

infrared spectroscopy. **c**, Change in the concentration of reaction components over the reaction time course, monitored by *in situ* infrared spectroscopy. **d**, Proposed catalytic cycle.

enantio-determining step(s), guided by the protonation–dealkylation Arbuzov mechanistic sequence. Evidence for the intermediacy of a protiophosphonium ion in the catalytic system was obtained by monitoring the reaction of **2a** with HCl catalysed by thiourea **1g** by ^{31}P NMR (Fig. 3a). At the earliest timepoints, the signal due to **2a** at δ 159 ppm is not observed, replaced instead by a doublet at δ 52 ppm that diminishes gradually with concomitant appearance of product **3a** at δ 24 ppm (Supplementary Fig. 2). The transient signal at δ 52 is assigned to the phosphonium chloride intermediate **6a** based on the 710 Hz ($J_{\text{P}-\text{H}}$) coupling constant³² and the spectrum of an independently prepared phosphonium tetrafluoroborate (Supplementary Fig. 1). These observations indicate that phosphonium chloride **6a** is the resting state of the substrate under the catalytic conditions.

The resting-state form of catalyst **1g** was investigated by using diffusion-ordered NMR spectroscopy (DOSY) to measure its diffusion constant under catalytic reaction conditions as a means of estimating its molecular weight (Supplementary Information section 8.2). The trifluoromethyl groups on **1g** provided a sensitive handle for ^{19}F NMR measurements at concentrations of **1g** appropriate to the catalytic conditions (10 mM, 5% Et₂O/toluene- d_8 , -70°C). After calibration studies³³, we established that a solution of catalyst **1g** alone affords a measured molecular weight that is consistent with a monomeric state ($\text{MW}_{\text{det}} = 640$, $\text{MW}(\mathbf{1g}) = 646$, $\Delta\text{MW} = 1\%$). Under reaction conditions that reliably afford high yield and enantioselectivity, the measured molecular weight of the catalyst resting state is consistent with a 1:1 **1g** · **6a** complex ($\text{MW}_{\text{det}} = 1,043$, $\text{MW}(\mathbf{1g} \cdot \mathbf{6a}) = 1,005$, $\Delta\text{MW} = -4\%$) (Fig. 3b). On completion of the reaction, the measured molecular weight is intermediate between that of monomeric **1g** and a 1:1 **1g** · **3a** complex ($\text{MW}_{\text{det}} = 739$, $\text{MW}(\mathbf{1g} \cdot \mathbf{3a}) = 878$, $\text{MW}(\mathbf{1g}) = 646$, $\Delta\text{MW} = 16\%$ or -14%), consistent with an equilibrium between free and product-bound catalyst, and inconsistent with strong catalyst–product binding. These observations establish that catalyst **1g** rests as a 1:1 complex with phosphonium **6a** and that rate-limiting dealkylation proceeds from this complex.

With the molecular composition of the resting-state complex established, we attempted to determine the kinetic dependence on $[\mathbf{1g}]_T$ and $[\mathbf{6a}]$ to elucidate the stoichiometry of the rate-determining transition-state complex (Fig. 3b). The distinct infrared absorbance of the $P=O$ bond in **3a** ($1,240\text{ cm}^{-1}$) and the symmetric $P-O$ stretch in **6a** ($1,039\text{ cm}^{-1}$) provided excellent handles to monitor reaction progress by *in situ* infrared spectroscopy. By systematically varying the concentration of **1g** and applying the normalized time scale treatment to the reaction profiles as in ref. 34, we obtained excellent graphical overlay only when dividing the reaction profiles by $[\mathbf{1g}]^n$ for $n = 1$, indicating that the reaction rate exhibits first-order dependence on catalyst $[\mathbf{1g}]_T$. Furthermore, the consumption of phosphonium species **6a** and the formation of product **3a** both follow a zeroth-order kinetic rate behaviour for approximately 80% of the reaction (Fig. 3c), consistent with a turnover-limiting and enantiodetermining dealkylation transition state proceeding from a 1:1 **1g** · **6a** resting-state complex.

A catalytic cycle consistent with all available mechanistic data is shown in Fig. 3d. This cycle features (1) a protonation equilibrium that favours the phosphonium chloride **6a**; (2) binding of **6a** to monomeric catalyst **1g** forming the resting state; and (3) turnover-limiting and enantiodetermining dealkylation to form product **3a** and benzyl chloride, which dissociate from the catalyst to turn over the catalytic cycle.

Computational analysis

The relatively small size of catalyst **1g** rendered the S_N2 step amenable to explicit modelling by density functional theory. Modelling of the catalysed and uncatalysed dealkylation reactions of phosphonium chloride **6a** was performed with continuum solvation in a low dielectric (PCM, toluene, $\epsilon = 2.38$) to mimic the experimental reaction conditions (Fig. 4a). The interactions between the catalyst and the phosphonium chloride were further analysed using the independent gradient model based on Hirshfeld partition (IGMH) (Supplementary Information

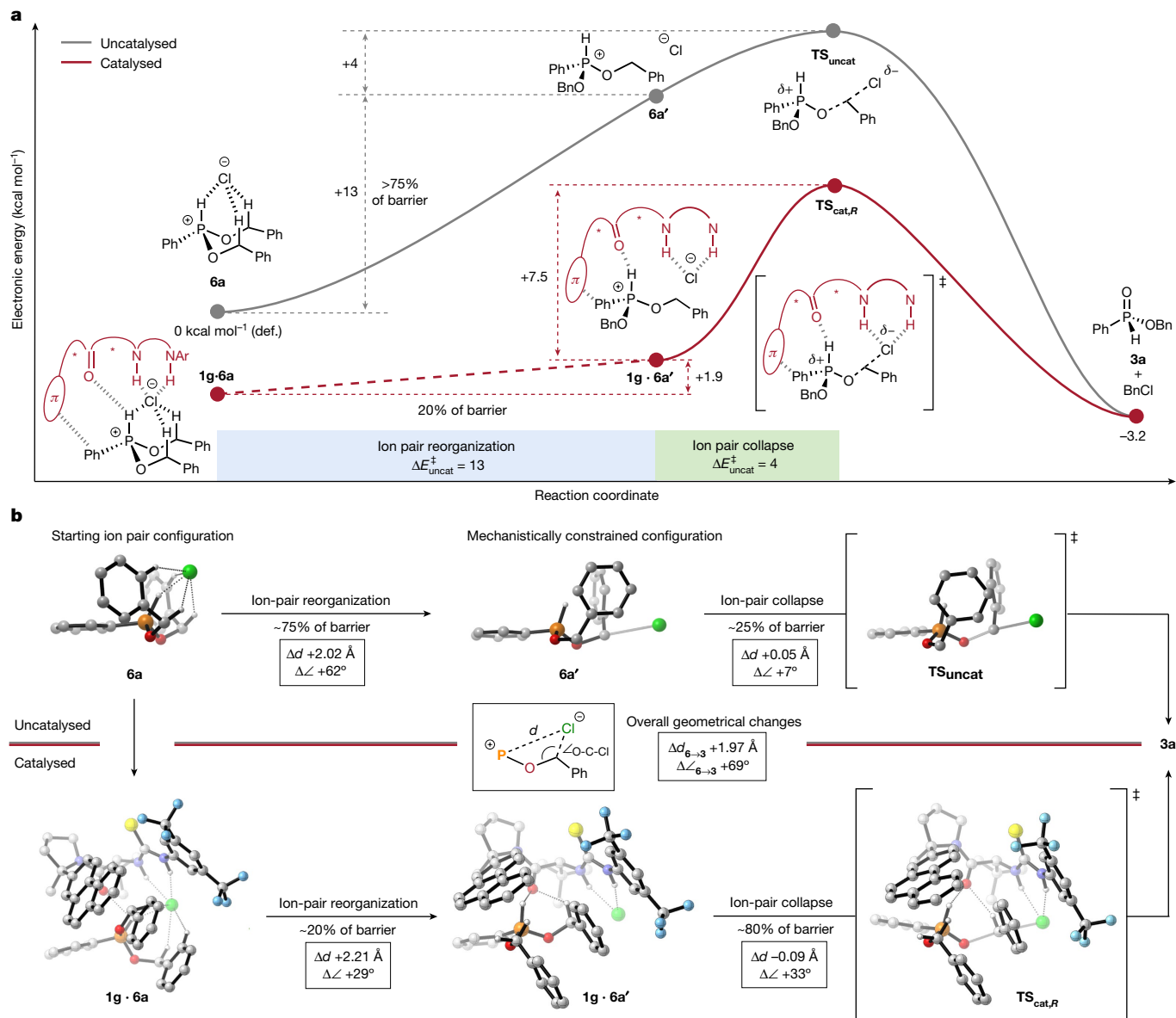


Fig. 4 | Origins of catalytic rate acceleration. All calculations were performed at the B3LYP-D3/6-311++G(d,p)/PCM(Toluene)//B3LYP-D3/def2-SVP/PCM(Toluene) level of theory at 195.15 K and 1 atm. Most hydrogens are hidden for clarity. **a**, Calculated potential energy surfaces for uncatalysed background (grey) and catalysed (red) pathways. Species **6a'** is a non-stationary state structure

corresponding to maximum P–Cl separation on the intrinsic reaction coordinate of the background reaction. The reported values are electronic energies without zero-point vibrational corrections. **b**, Graphical representation of key reaction species and geometrical changes associated with the reorganization and collapse phases of the catalysed and uncatalysed pathways.

section 10.4). In the absence of a catalyst, the phosphonium chloride **6a** is found to rest as a tight ion pair with a cage-like structure in which the chloride anion engages in multiple stabilizing interactions with the cation. All of the stabilizing H-bonding interactions and a substantial portion of the Coulombic attraction present in the ground state must be sacrificed, in a manner loosely analogous to desolvation from the aqueous medium in the halogenase reaction, to attain the linear geometry mandated by the S_N2 mechanism as in **TS_{uncat}** (ref. 35). In considering this geometric reorganization, the concerted pathway for dealkylation can be partitioned conceptually into an ion-pair reorganization phase followed by an ion-pair collapse phase. These two phases can be demarcated by a non-stationary state **6a'** located on the computed intrinsic reaction coordinate, in which the chloride ion is positioned along the S_N2 trajectory but formation of the C–O bond has yet to commence. By this analysis, >75% of the overall electronic activation barrier results from reorganization of the chloride anion in the first phase (**6a** → **6a'**),

whereas the ion-pair collapse phase corresponding to the covalent bond-breaking and forming events contributes less than 25% (about 4 kcal mol⁻¹) to the overall barrier.

In the computational model of the catalysed pathway, the nucleophilic substitution was found to proceed in two discrete steps (Fig. 4a). Three critical points along the reaction coordinate may be distinguished: binding of **1g** to the ion pair **6a**, the reorganized ion pair **6a'** and the transition state of the dealkylation step. In all three structures, the catalyst engages in a network of stabilizing noncovalent interactions with both cationic and anionic components of the phosphonium chloride ion pair (Extended Data Fig. 1, bottom), in agreement with the previous studies on thiourea–arylpiperidine scaffolds²². The chloride binds to the thiourea and the phosphonium associates with the arylpiperidine domain. These interactions seem to stabilize both charged components of the ion pair. From the resting-state complex **1g · 6a**, a structure **1g · 6a'** could be located as a stationary state only

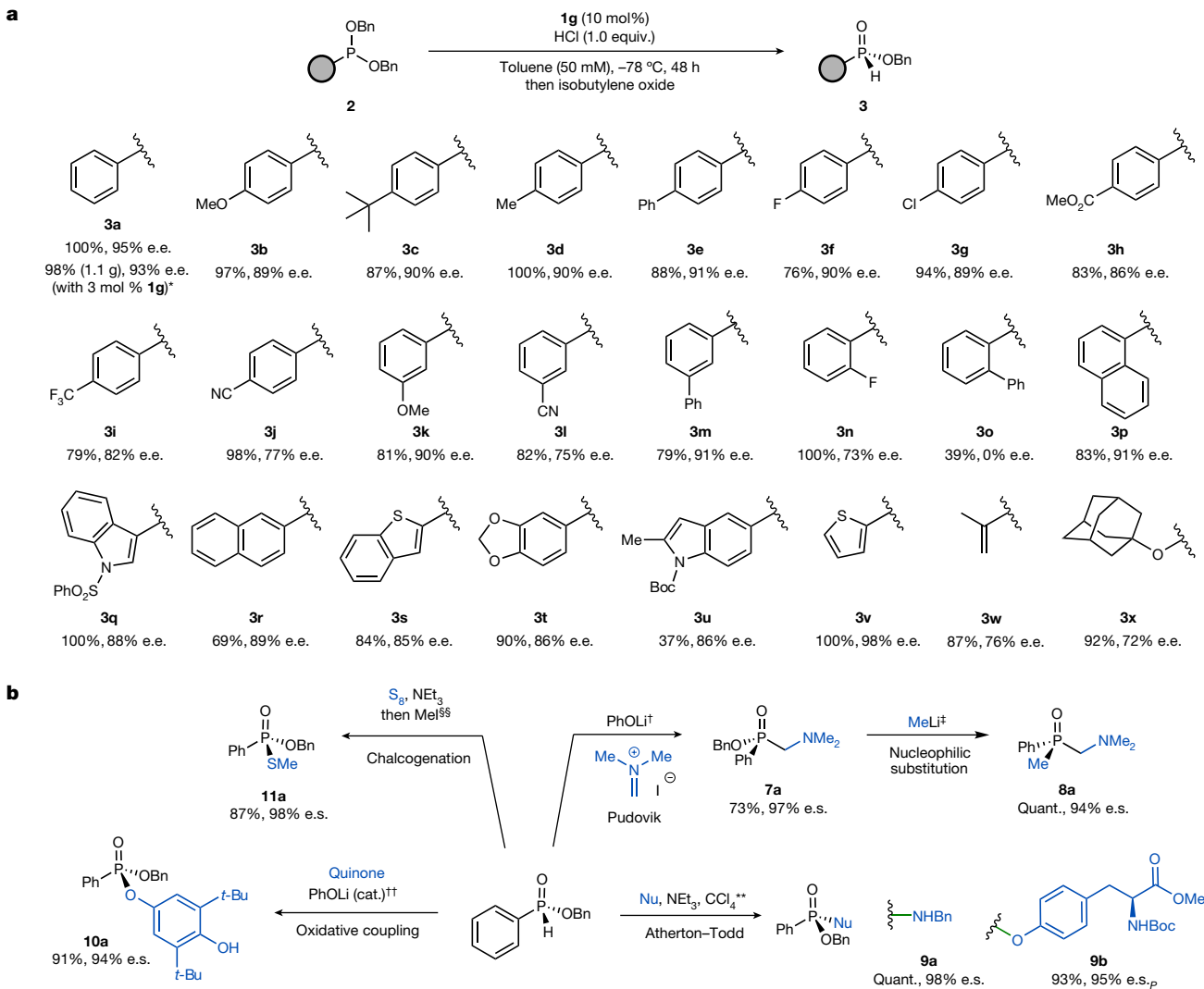


Fig. 5 | Enantioselective phosphonium dealkylation of phosphonites and stereospecific elaborations of H-phosphinate products. All reported yields are of chromatographically purified and isolated material. **a**, Substrate scope. Reactions were conducted with 0.1 mmol of phosphonite. **b**, Stereospecific elaborations. Enantiospecificity (e.s.) is defined as $e.e._{product}/e.e._{reactant}$. *Reaction was conducted with 5 mmol **2a**. No isobutylene oxide quench was employed, and 95% of catalyst **1g** was recovered from column chromatography.

†Eschenmoser's salt (1.0 equiv.), PhOLi (1 equiv.), THF, -40°C , 17 h. ‡MeLi (1.5 equiv., 1.6 M in Et_2O), THF, -78°C , 30 min, then 0°C , 90 min. §Benzophenone (1.0 equiv.), PhOLi (20 mol%), THF, -40°C , 16 h. **Nucleophile (2.0 equiv.), Et_3N (2.0 equiv.), CCl_4 (2.0 equiv.), Et_2O , 0°C to rt, 7 h. ††2,6-di-*tert*-butyl-1,4-benzoquinone (1.0 equiv.), PhOLi (20 mol%), THF, -40°C , 16 h. §§ S_8 (1.5 equiv.), Et_3N (1.05 equiv.), Et_2O , 0°C to room temperature, 24 h, then MeI (2.0 equiv.), Et_2O , room temperature, 2 h.

1.9 kcal mol^{-1} uphill, which is on the intrinsic reaction coordinate to the lowest-energy transition state $\text{TS}_{\text{cat},R}$ (see below).

Remarkably, the geometrical features of the phosphonium chloride resting-state complex **1g** · **6a'** are very similar to those in **6a'**, that is, the chloride is positioned by hydrogen bonding in a nearly optimal pre-transition-state geometry (Fig. 4b), primed to enter $\text{TS}_{\text{cat},R}$. Thus, catalyst **1g** can be seen as engaging a network of attractive noncovalent interactions to access a relatively stable ground-state complex **1g** · **6a'** that is primed for the dealkylation reaction. The computational analysis enables a quantitative assessment of the effect of catalyst **1g** on both the ion-pair reorganization and the ion-pair collapse. Catalyst association raises the barrier to ion-pair collapse relative to the uncatalysed pathway (7.5 kcal mol^{-1} versus 4.0 kcal mol^{-1} ; Fig. 4a), consistent with the expected attenuating effect of H-bonding on the nucleophilicity of chloride. However, inhibition of ion-pair collapse is more than offset by the catalyst mitigating the energetic cost of the requisite geometric preorganization of the phosphonium chloride ion pair (1.9 kcal mol^{-1} versus 13 kcal mol^{-1} ;

Fig. 4a), resulting in overall acceleration relative to the background reaction.

Origin of enantioinduction

A systematic conformer search led to the identification of low-energy diastereomeric structures leading to the major (*R*) and minor (*S*) enantiomers of **3a**, with relative energies in excellent agreement with the experimentally observed enantioselectivities. A close analysis of the computational models with the IGMH approach³⁶ (Supplementary Fig. 14) shows specific stabilizing interactions that might be responsible for enantioinduction. The diastereomeric transition-state structures leading to the minor (*S*) and major (*R*) product enantiomers show almost identical catalyst geometries but are related by a 120° rotation of the phosphonium ions in the catalyst active site. $\text{TS}_{\text{cat},S}$ positions the phosphonium *P*-Ph group below the 2-phenanthryl group of the catalyst, while splaying its benzyl groups (highlighted green). The lower energy $\text{TS}_{\text{cat},R}$, in contrast, positions the phosphonium *P*-Ph group into

solvent and stacks the two benzyloxy groups, with one residing below the 2-phenanthryl group of the catalyst. Although **TS_{cat,S}** and **TS_{cat,R}** both possess several noncovalent attractive interactions in common, **TS_{cat,S}** possesses an additional H-bonding interaction between a benzylic C–H and the amide oxygen (Extended Data Fig. 1, orange box) whereas **TS_{cat,R}** incorporates two benzylic C–H–π interactions in (Extended Data Fig. 1, blue box). The net energetic benefit of losing one benzylic C–H hydrogen bonding interaction and gaining two benzylic C–H–π interactions is thus proposed to play a key part in dictating the sense and magnitude of enantioinduction³⁷.

Substrate scope development and product derivatization

Finally, we examined the substrate scope of our discovered protocol, recognizing that the stereocontrolled synthesis of stereogenic at-phosphorus compounds is a topic of considerable current interest^{29–31}. A wide array of dibenzyl phosphonites proved compatible as substrates, furnishing air- and moisture-stable chiral *H*-phosphinate products that can be purified by silica gel column chromatography (Fig. 5a). Various *para*-substituted arylphosphonites underwent dealkylation with good yield and enantioselectivity (**3a**–**3g**), with lower enantioselectivity observed for substrates bearing highly electron-withdrawing substituents (**3h**–**3j**). *Meta*-substituted phenylphosphonites underwent dealkylation with comparable enantioselectivities to their *para*-substituted regiosomers (**3k**–**3m**). By contrast, sterically demanding *ortho* substituents proved deleterious for enantioselectivity: *o*-fluoro substitution decreased enantioselectivity from 90% (**3f**) to 73% e.e. (**3n**), whereas *o*-phenyl substitution ablated enantioselectivity (**3o**). Substrates bearing *ortho*-fused polyaromatic substituents, however, underwent dealkylation with high enantioselectivity (**3p** and **3q**). The method is also compatible with a variety of hetero- and polyaromatic substituents (**3r**–**3t** and **3v**), including acid-labile functional groups (*N*-Boc-protected indole, **3u**). Phosphonites with non-aryl substituents such as isopropenyl (**3w**) and adamantlyoxy (**3x**) underwent dealkylation with moderate levels of enantioselectivity, whereas alkyl substituents such as cyclopropyl and methyl afforded low levels of enantioselectivity at 54% and 30% e.e., respectively (Supplementary Information section 3). The enantioselective dealkylation of **2a** was performed successfully on a gram scale using only 3 mol% **1g** with high enantioselectivity (93% e.e.), yield (98%) and efficient catalyst recovery (95%).

Most notably, this *proto*-Michaelis–Arbuzov reaction yields enantioenriched *H*-phosphinates, *P*-stereogenic building blocks with broad synthetic utility but that are currently accessible only by stoichiometric approaches or kinetic resolution^{29,38,39}, differentiating our approach from previous catalytic approaches that desymmetrize a P(V) compound by nucleophilic substitution^{40,41}. The substituents on the *H*-phosphinate products obtained through this enantioselective dealkylation are known to exhibit complementary reactivity as the proton and alkoxide groups on phosphorus are prone to substitution by electrophiles and nucleophiles, respectively²⁹. To highlight the synthetic utility of enantioenriched *H*-phosphinates, we explored the reactivity of (*R*)-benzyl phenylphosphinate **3a** as an orthogonally bifunctionalizable *P*-stereogenic building block. We found it amenable to an array of stereospecific synthetic elaborations of the *P*–H moiety, followed by secondary derivatization of the *P*–OBn moiety (Fig. 5b). Building on established phospha-Mannich reactivity of phosphinates⁴², we found that deprotonation with lithium phenoxide enabled **3a** to participate in the Pudovik addition to Eschenmoser's salt⁴³, affording α-amino phosphinate **7a**. The benzyloxy group of **7a** could subsequently be substituted in the presence of methylolithium to afford **8a**, preserving enantioenrichment at phosphorus^{44–46}. We also explored a polarity reversal strategy in the context of the Atherton–Todd reaction⁴⁷, in which the nucleophilic *P*–H moiety was converted to electrophilic *P*–Cl

and then trapped with heteroatom-based nucleophiles. In this context, nucleophiles such as benzylamine and tyrosine could be used to access phosphonate esters and phosphonamides **9a** and **9b** with high yields and enantiospecificities. To investigate phosphoryl-radical-mediated reactivity, we adapted the lithium phenoxide conditions to a previously reported 1,6-coupling between *H*-phosphinates and benzoquinones⁴⁸, finding that *O*-phosphoryl hydroquinone derivative **10a** was obtained with excellent stereospecificity. This result indicates that the **3a**-derived phosphoryl radical possesses sufficient configurational stability in the absence of chiral control elements to engage in stereospecific reactions⁴⁹. Finally, **3a** was subjected to a sulfuration–methylation sequence to afford phosphonothioate **11a** with excellent enantiospecificity⁵⁰.

Outlook

Precise preorganization of reactants in a favourable pre-transition-state geometry, a mechanistic principle fundamental in enzyme catalysis but hitherto unexploited in small-molecule systems, has now been developed and characterized in the context of an HBD catalyst for enantioselective Michaelis–Arbuzov reactions that generate valuable *P*-stereogenic products and building blocks. The mechanistic scenario characterized here recapitulates the energetic origin for FDAS catalysis in a small-molecule model. We anticipate that this demonstration of the geometric preorganization principle in a small-molecule system will be broadly relevant to the catalysis of ionic pathways in which ion-pair reorganization is an important component of the turnover-limiting reaction barrier.

Online content

Any methods, additional references, Nature Portfolio reporting summaries, source data, extended data, supplementary information, acknowledgements, peer review information; details of author contributions and competing interests; and statements of data and code availability are available at <https://doi.org/10.1038/s41586-024-07811-4>.

- Anslyn, E. V. & Dougherty, D. A. in *Modern Physical Organic Chemistry* 637–670 (Univ. Science Books, 2005).
- O'Hagan, D. & Schmidberger, J. W. Enzymes that catalyse S_n2 reaction mechanisms. *Nat. Prod. Rep.* **27**, 900–918 (2010).
- Dewar, M. J. S. New ideas about enzyme reactions. *Enzyme* **36**, 8–20 (2017).
- Agarwal, V. et al. Enzymatic halogenation and dehalogenation reactions: pervasive and mechanistically diverse. *Chem. Rev.* **117**, 5619–5674 (2017).
- Parker, A. J. Protic-dipolar aprotic solvent effects on rates of bimolecular reactions. *Chem. Rev.* **69**, 1–32 (1969).
- Dong, C. et al. Crystal structure and mechanism of a bacterial fluorinating enzyme. *Nature* **427**, 561–565 (2004).
- Zhu, X., Robinson, D. A., McEwan, A. R., O'Hagan, D. & Naismith, J. H. Mechanism of enzymatic fluorination in *Streptomyces cattleya*. *J. Am. Chem. Soc.* **129**, 14597–14604 (2007).
- Senn, H. M., O'Hagan, D. & Thiel, W. Insight into enzymatic C–F bond formation from QM and QM/MM calculations. *J. Am. Chem. Soc.* **127**, 13643–13655 (2005).
- Warshel, A. et al. Electrostatic basis for enzyme catalysis. *Chem. Rev.* **106**, 3210–3235 (2006).
- Bruice, T. C. & Benkovic, S. J. Chemical basis for enzyme catalysis. *Biochemistry* **39**, 6267–6274 (2000).
- Uyeda, C. & Jacobsen, E. N. Transition-state charge stabilization through multiple non-covalent interactions in the guanidinium-catalyzed enantioselective Claisen rearrangement. *J. Am. Chem. Soc.* **133**, 5062–5075 (2011).
- Lin, S. & Jacobsen, E. N. Thiourea-catalysed ring opening of episulfonium ions with indole derivatives by means of stabilizing non-covalent interactions. *Nat. Chem.* **4**, 817–824 (2012).
- Taylor, M. S. & Jacobsen, E. N. Asymmetric catalysis by chiral hydrogen-bond donors. *Angew. Chem. Int. Ed.* **45**, 1520–1543 (2006).
- Zhou, H. et al. Organocatalytic stereoselective cyanosilylation of small ketones. *Nature* **605**, 84–89 (2022).
- Metrano, A. J. et al. Asymmetric catalysis mediated by synthetic peptides, version 2.0: expansion of scope and mechanisms. *Chem. Rev.* **120**, 11479–11615 (2020).
- Taylor, M. S. & Jacobsen, E. N. Highly enantioselective catalytic acyl-Pictet–Spenger reactions. *J. Am. Chem. Soc.* **126**, 10558–10559 (2004).
- Taylor, M. S., Tokunaga, N. & Jacobsen, E. N. Enantioselective thiourea-catalyzed acyl–Mannich reactions of isoquinolines. *Angew. Chem. Int. Ed.* **44**, 6700–6704 (2005).
- Doyle, A. G. & Jacobsen, E. N. Small-molecule H-bond donors in asymmetric catalysis. *Chem. Rev.* **107**, 5713–5743 (2007).

19. Brak, K. & Jacobsen, E. N. Asymmetric ion-pairing catalysis. *Angew. Chem. Int. Ed.* **52**, 534–561 (2013).
20. Zuend, S. J. & Jacobsen, E. N. Mechanism of amido-thiourea catalyzed enantioselective imine hydrocyanation: transition state stabilization via multiple non-covalent interactions. *J. Am. Chem. Soc.* **131**, 15358–15374 (2009).
21. Pupo, G. et al. Hydrogen bonding phase-transfer catalysis with potassium fluoride: enantioselective synthesis of β -fluoroamines. *J. Am. Chem. Soc.* **141**, 2878–2883 (2019).
22. Strassfeld, D. A. & Jacobsen, E. N. in *Supramolecular Catalysis* (eds van Leeuwen, P. W. N. M. & Raynal, M.) 361–385 (Wiley, 2022).
23. Bhattacharya, A. K. & Thyagarajan, G. Michaelis–Arbuzov rearrangement. *Chem. Rev.* **81**, 415–430 (1981).
24. Razumov, A. I. Mechanism of the Arbuzov rearrangement. *Zh. Obshch. Khim.* **29**, 1635–1639 (1959).
25. Razumov, A. I. & Bankovskaya, N. N. Preparation and some properties of intermediate products of the Arbuzov rearrangement. *Dokl. Akad. Nauk BSSR* **116**, 241 (1957).
26. Appel, R. Tertiary phosphane/tetrachloromethane, a versatile reagent for chlorination, dehydration, and P–N linkage. *Angew. Chem. Int. Ed. Engl.* **14**, 801–811 (1975).
27. Staudinger, H. & Meyer, J. Über neue organische Phosphorverbindungen III. Phosphinmethylenderivate und Phosphinimine. *Helv. Chim. Acta* **2**, 635–646 (1919).
28. Niland, C. J., Ruddy, J. J., O’Fearraigh, M. P. & McGarrigle, E. M. Asymmetric organocatalyzed synthesis of α -aminophosphinates via thiourea anion-binding catalysis. *Eur. J. Org. Chem.* **27**, e202301212 (2024).
29. Lemouzy, S., Giordano, L., Héault, D. & Buono, G. Introducing chirality at phosphorus atoms: an update on the recent synthetic strategies for the preparation of optically pure *P*-stereogenic molecules. *Eur. J. Org. Chem.* **2020**, 3351–3366 (2020).
30. Ye, X., Peng, L., Bao, X., Tan, C.-H. & Wang, H. Recent developments in highly efficient construction of *P*-stereogenic centers. *Green Synth. Catal.* **2**, 6–18 (2021).
31. Liu, J., Chen, H., Wang, M., He, W. & Yan, J.-L. Organocatalytic asymmetric synthesis of *P*-stereogenic molecules. *Front. Chem.* **11**, 1132025 (2023).
32. Kühl, O. in *Phosphorus-31 NMR Spectroscopy: A Concise Introduction for the Synthetic Organic and Organometallic Chemist* (ed. Kühl, O.) 7–23 (Springer, 2008).
33. Neufeld, R. & Stalke, D. Accurate molecular weight determination of small molecules via DOSY-NMR by using external calibration curves with normalized diffusion coefficients. *Chem. Sci.* **6**, 3354–3364 (2015).
34. Burés, J. A simple graphical method to determine the order in catalyst. *Angew. Chem. Int. Ed.* **55**, 2028–2031 (2016).
35. Shaik, S. S. in *Progress in Physical Organic Chemistry* (ed. Taft, R. W.) 197–337 (1985).
36. Lu, T. & Chen, Q. Independent gradient model based on Hirshfeld partition: A new method for visual study of interactions in chemical systems. *J. Comput. Chem.* **43**, 539–555 (2022).
37. Nishio, M. The CH/ π hydrogen bond in chemistry. Conformation, supramolecules, optical resolution and interactions involving carbohydrates. *Phys. Chem. Chem. Phys.* **13**, 13873–13900 (2011).
38. Gatineau, D. et al. H-adamantylphosphinates as universal precursors of *P*-stereogenic compounds. *J. Org. Chem.* **80**, 4132–4141 (2015).
39. Fu, X. et al. Chiral guanidinium salt catalyzed enantioselective phospha-Mannich reactions. *Angew. Chem. Int. Ed.* **48**, 7387–7390 (2009).
40. Forbes, K. C. & Jacobsen, E. N. Enantioselective hydrogen-bond-donor catalysis to access diverse stereogenic-at-*P*(V) compounds. *Science* **376**, 1230–1236 (2022).
41. Formica, M. et al. Catalytic enantioselective nucleophilic desymmetrization of phosphonate esters. *Nat. Chem.* **15**, 714–721 (2023).
42. Kolodiazhnaya, A. O. & Kolodiaznyi, O. I. Catalytic asymmetric synthesis of C-chiral phosphonates. *Symmetry* **14**, 1758 (2022).
43. Yamagishi, T. et al. Diastereoselective synthesis of β -substituted α -hydroxyphosphinates through hydrophosphinylation of α -heteroatom-substituted aldehydes. *Tetrahedron* **59**, 767–772 (2003).
44. Xu, Q., Zhao, C.-Q. & Han, L.-B. Stereospecific nucleophilic substitution of optically pure *H*-phosphinates: a general way for the preparation of chiral *P*-stereogenic phosphine oxides. *J. Am. Chem. Soc.* **130**, 12648–12655 (2008).
45. Han, Z. S. et al. General and stereoselective method for the synthesis of sterically congested and structurally diverse *P*-stereogenic secondary phosphine oxides. *Org. Lett.* **19**, 1796–1799 (2017).
46. Gatineau, D., Giordano, L. & Buono, G. Bulky, optically active *P*-stereogenic phosphine-boranes from pure *H*-menthylphosphinates. *J. Am. Chem. Soc.* **133**, 10728–10731 (2011).
47. Xiong, B. et al. Systematic study for the stereochemistry of the Atherton–Todd reaction. *Tetrahedron* **69**, 9373–9380 (2013).
48. Xiong, B., Shen, R., Goto, M., Yin, S.-F. & Han, L.-B. Highly selective 1,4- and 1,6-addition of *P*(O)₃-H compounds to *p*-quinones: a divergent method for the synthesis of C- and O-phosphoryl hydroquinone derivatives. *Chem. Eur. J.* **18**, 16902–16910 (2012).
49. Han, L.-B. & Zhao, C.-Q. Stereospecific addition of *H*-P bond to alkenes: a simple method for the preparation of (*R*_p)-phenylphosphinates. *J. Org. Chem.* **70**, 10121–10123 (2005).
50. Wang, W.-M. et al. Stereospecific preparations of *P*-stereogenic phosphonothioates and phosphonoselenoates. *J. Org. Chem.* **81**, 6843–6847 (2016).

Publisher’s note Springer Nature remains neutral with regard to jurisdictional claims in published maps and institutional affiliations.

Springer Nature or its licensor (e.g. a society or other partner) holds exclusive rights to this article under a publishing agreement with the author(s) or other rightsholder(s); author self-archiving of the accepted manuscript version of this article is solely governed by the terms of such publishing agreement and applicable law.

© The Author(s), under exclusive licence to Springer Nature Limited 2024

Article

Data availability

The data that support the findings in this work are available in the paper and in the Supplementary Information.

Acknowledgements This work was supported by the National Institutes of Health through grant nos. GM043214 and GM 149244, and F32 postdoctoral fellowship (GM136042) to G.J.L. We thank D. Cui and A. Lowe (Harvard University) for assistance with the NMR experiments, and J. Gair, M. Isomura and S. Nistanaki for their helpful discussions.

Author contributions G.J.L. and E.N.J. conceived the work; G.J.L. and M.H.S. designed and conducted the experiments; E.N.J. supervised and directed the research; and all authors wrote the paper.

Competing interests The authors declare no competing interests.

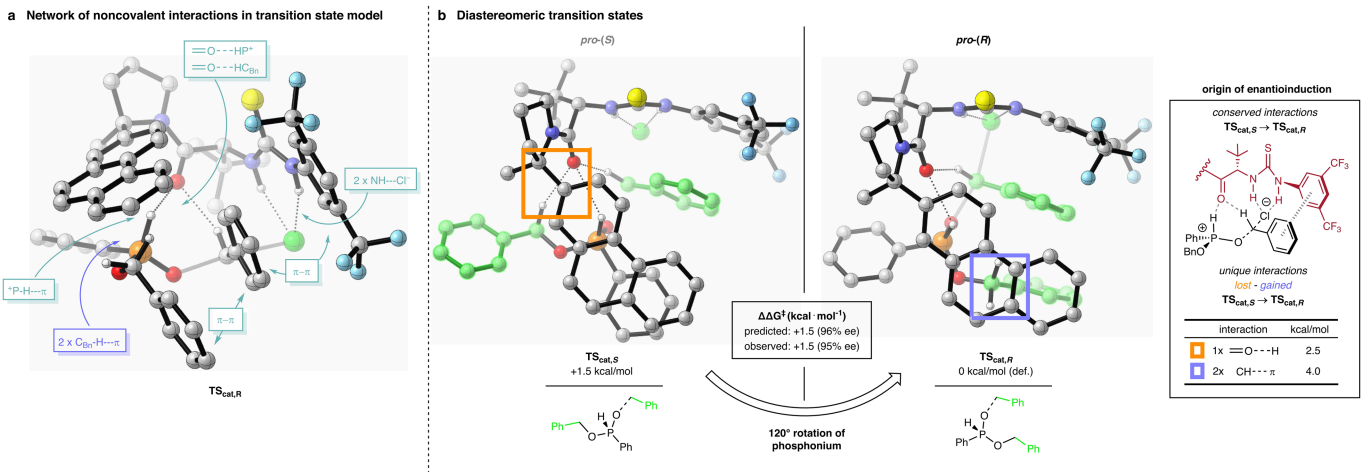
Additional information

Supplementary information The online version contains supplementary material available at <https://doi.org/10.1038/s41586-024-07811-4>.

Correspondence and requests for materials should be addressed to Eric N. Jacobsen.

Peer review information *Nature* thanks the anonymous reviewers for their contribution to the peer review of this work.

Reprints and permissions information is available at <http://www.nature.com/reprints>.



Extended Data Fig. 1 | Origins of enantioselectivity. All calculations were performed at the B3LYP-D3/6-311++G(d,p)/PCM(toluen) e //B3LYP-D3/def2-SVP/PCM(toluen) level of theory at 195.15 K and 1 atm. Most hydrogens are hidden for clarity. **(A)** Analysis of non-covalent interactions **(B)** Density-functional-

theory-modeled diastereomeric transition states for dealkylation with highlighted differential stabilizing interactions hypothesized to be the origin of enantioinduction.